Title:

Analysis of Scavenge Port Designs and Exhaust Valve Profiles on the In-cylinder Flow and Scavenging Performance in a 2-Stroke Boosted Uniflow Scavenged Direct Injection Gasoline (BUSDIG) Engine

Author names and affiliations:

Xinyan Wang *, Jun Ma and Hua Zhao

Centre for Advanced Powertrain and Fuels, Brunel University London, Uxbridge UB8 3PH, United Kingdom.

* Corresponding author: Tel: +44 01895 265903, Email: xinyan.wang@brunel.ac.uk.

Abstract:

In this study, effects of intake scavenge port designs and exhaust valve opening profiles were studied on the scavenging process in a newly proposed 2-stroke boosted uniflow scavenged direct injection gasoline (BUSDIG) engine by detailed three dimensional engine simulations. As the most important geometric parameters, the axis inclination angle (AIA) and swirl orientation angle (SOA) of scavenge ports, as shown in Figure 1, were investigated and optimized for best scavenging performances at first. With the optimal AIA of 90^0 and SOA of 20^0, various combinations of scavenge port opening (SPO) timing, exhaust valve opening duration (ED) and exhaust valve opening (EVO) timing were then analysed. Four distinct scavenging periods, i.e. early backflow period (EB), backflow scavenging period (BS), main scavenging period (MS) and post backflow period (PB), were identified and their impacts on the in-cylinder flow motions and scavenging performances were investigated. The results show that the optimal scavenging performance can be achieved with a higher delivery ratio (DR), charging efficiency (CE) and scavenging efficiency (SE) when the post backflow is

just avoided by tuning the difference between the closing timings of scavenge ports and exhaust valves (Δ_{close}) and the overlap between the opening profiles of scavenge ports and exhaust valves ($\Delta_{overlap}$) for a specific ED. A longer ED can be used to further improve the scavenging performances. In addition, the difference between the opening timings of scavenge ports and exhaust valves (Δ_{open}) can be increased to improve SE. The Δ_{close} also shows strong positive correlation with in-cylinder swirl ratio (SR) and negative correlation with tumble ratio (TR). The results presented in this study provide the fundamental knowledge of the scavenging process in the uniflow scavenged 2-stroke engine and assist the design of scavenge ports and valve strategies to optimize in-cylinder flow motion and scavenge performances in the 2-stroke BUSDIG engine with a variable valve actuation system for exhaust valves.

Keywords: computational fluid dynamics, 2-stroke engine, uniflow, scavenging process, variable valve actuation.

1. Introduction

The engine down-sizing and down-speeding technologies show great potential to improve the fuel consumption of the automotive engine. Compared to the 4-stroke engine, the compact 2-stroke engine doubles the firing frequency and operates at a lower indicated mean effective pressure (IMEP) at the same torque. The adoption of the direct injection after exhaust valve closing avoids the fuel short-circuiting, which in turn lowers the fuel consumption and pollutant emissions dramatically. In addition, the fuel consumption in a 2-stroke engine can be further improved with lean/stratified charge achieved by direct injection [1-4] and advanced combustion concept [5-10], e.g. controlled auto-ignition (CAI), partially premixed combustion (PPC) and reactivity-controlled compression ignition (RCCI).

The scavenging process in a 2-stroke engine directly controls the in-cylinder flow motion, charge mixture formation and the subsequent combustion performance. During the 2-stroke scavenging process, the fresh intake charge scavenges the burnt gases out of the cylinder and fills the cylinder for the next cycle. However, the conventional 2-stroke engines suffer from the fuel/air short-circuiting phenomenon, in which some of the intake fresh mixture would flow directly into the exhaust port during the scavenging process [11], due to the large overlapping period of intake and exhaust process. Compared to the cross and loop scavenge engines, the uniflow scavenged 2-stroke engine shows superior scavenging performance [12]. The intake scavenge ports in a uniflow scavenged engine are integrated to the cylinder liner and controlled by the movement of piston top while exhaust valves are placed in the cylinder head. Therefore, the bore distortion caused by uneven thermal loading in the conventional ported 2-stroke engine could be minimized in the uniflow scavenged engine. In addition, this layout enables the application of variable valve actuation (VVA) technology to adjust the exhaust valve timings/durations and hence the scavenging process under different operating conditions.

The uniflow scavenged 2-stroke engines have been mostly used in large marine diesel engines [13-15] and recently researched for their potential applications to passenger cars [3, 10, 12, 16-19]. They are characterized by the strong swirl flow motion formed by the angled intake scavenge ports at the bottom of cylinder liner [20-22]. The axis inclination angle (AIA) and swirl orientation angle (SOA) are shown to have most impact on the in-cylinder flow motions and the scavenging performances in the uniflow scavenged 2-stroke engine [23]. Tamamidis and Assanis [24] investigated the effect of SOA on in-cylinder flow motions in a 2-stroke scavenged engine by computational fluid dynamics (CFD) simulations of one sector of the cylinder (including one inlet port) and found the larger swirl angles of the inlet ports produce higher swirl levels inside the cylinder. Laget et al. [18] performed the CFD simulations to optimize the swirl orientation angle of scavenge ports in a 2-stroke uniflow diesel engine and found the reduction of swirl orientation angle from 17 to 10° produced an acceptable swirl motion intensity and a good scavenging performance. In addition to the scavenge port angles, the opening timing of the scavenge ports, which is determined by the upper edge of scavenge ports, and the exhaust valve lift profile also affect the scavenging process. Ravi and Marathe [25] found that extended intake scavenging process produced by early opening and late closing of the scavenge ports resulted in a higher scavenge ratio and scavenging efficiency but a lower trapping efficiency. It was also found the exhaust valve closing timing had little effect on the scavenging process, as long as the timings of intake and exhaust closing are not far apart. A multi-objective optimization of several design and operation engine parameters was performed for a 2-stroke supercharged uniflow scavenged diesel engine by Carlucci et al. [26]. They found the intake scavenge port opening timings together with the exhaust valves opening and closing timings were significant in determining the trapping and scavenging efficiencies, as well as the engine specific fuel consumption. Laget et al. [18] investigated the scavenging characteristics with different exhaust valve lifts

and timings and concluded that reducing the exhaust valve lift decreased the short-circuiting and an optimal valve lift may exists to achieve a good trade-off between a good scavenging and a reduced short-circuiting.

As indicated by the above literature review, the scavenge port designs (port angles and opening timing) and the exhaust valve opening profiles show significant impact on the in-cylinder flow motions and scavenge performances which would directly determine the combustion performances of the 2-stroke uniflow scavenged engine. In this study, the three dimensional (3D) computational fluid dynamics (CFD) simulations were performed to understand the effects of scavenge port angles, i.e. axis inclination angle (AIA) and swirl orientation angle (SOA), the scavenge port opening timings and exhaust valve opening profiles on the in-cylinder flow motions and scavenge performances in the proposed boosted uniflow scavenged direct injection gasoline (BUSDIG) engine [27, 28]. The analysis of the scavenging process with different AIA and SOA was carried out at first to determine the optimal scavenge port angles for the BUSDIG engine. Based on the optimal design of scavenge port angles, the simulations with various combinations of scavenge port opening (SPO) timing, exhaust valve opening duration (ED) and exhaust valve opening (EVO) timing were then performed to understand their impacts on in-cylinder flow motions and scavenge performances. The results presented in this study provide the fundamental knowledge of the scavenging process in the uniflow scavenged engine and assist the design of scavenge ports and valve strategies to optimize in-cylinder flow motion and scavenge performances in 2-stroke BUSDIG engine equipped with variable valve actuation (VVA) system for exhaust valves.

2. Specifications of the BUSDIG engine

Based on the initial design of bore/stroke for maximum performance [28], a pent roof cylinder head was incorporated in the BUSDIG engine to accommodate two exhaust valves, a

central mounted direct injection (DI) gasoline injector and spark plug. A shallow bowl was included in the centre of piston top to guide the fuel jets from injector and also avoid the interference with the spark plug. Considering the future application to multi-cylinder engines, two groups of scavenge ports (four on each side) were integrated to the cylinder respectively to avoid the interference of the scavenge ports on the adjacent cylinders. A single scavenge port occupies a 20^0 segment on the cylinder circumference and the interval between two adjacent scavenge ports in each group is fixed at 10^0. The interval between the two groups of scavenge ports is set at 70^0. The height of the scavenge ports was fixed at 14 mm. Fig. 1 shows schematically the design of the cylinder head and the piston bowl. The other engine specifications are shown in Table 1.

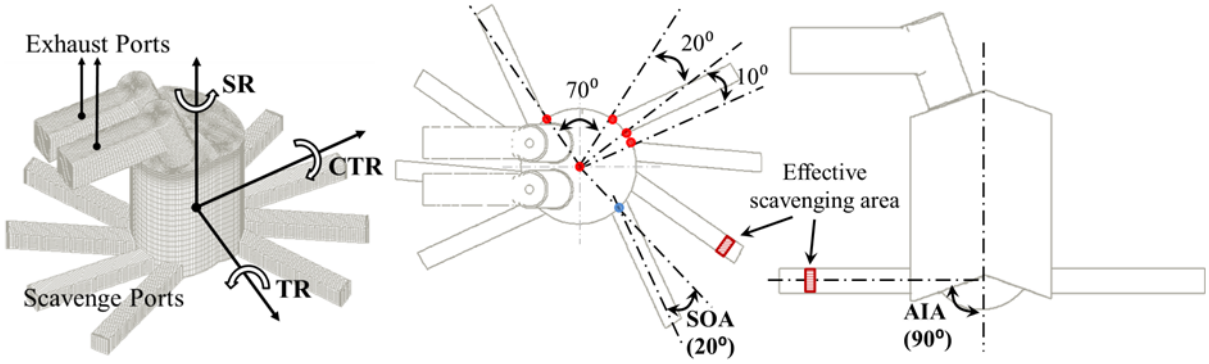

Fig. 1. Schematic diagram of the BUSDIG engine design.

Table 1. Engine specifications.

Bore	80 mm
Stroke	100 mm
Connecting rod	180 mm
Displacement	0.5 L
Compression ratio	14:1
Cylinder head	Pent roof / 2 exhaust valves
Piston	Bowl piston

In order to achieve optimal scavenge performance with current engine cylinder design, two key scavenge port angles, axis inclination angle (AIA) and swirl orientation angle (SOA), as shown in Fig. 1, were investigated and optimized at first. Then, the simulations with the optimal combination of AIA and SOA were performed to understand the effects of scavenge port/exhaust valve opening durations and timings on controlling the scavenging process in the 2-stroke BUSDIG engine by adjusting scavenge port opening (SPO) timing, exhaust valve duration (ED) and exhaust valve opening (EVO) timing. The locations and dimensions of scavenge ports on the cylinder liner and the port height were kept constant in this study. As the opening and closure of scavenge ports are symmetrical to the bottom dead centre (BDC), the adjustment of the scavenge port opening (SPO) timing would also change the scavenge port opening duration (SD).

3. Numerical models and simulation conditions

The commercial CFD software STAR-CD was adopted in this study to perform the simulations. Reynolds-Averaged Navier Stokes (RANS) approach was applied with RNG k-ε turbulence model in the simulations. The heat transfer was implemented through the general form of the enthalpy conservation equation for the fluid mixture. The Angelberger wall function was used for the simulation of the wall heat transfer. The detailed description of the numerical models can be found in Ref. [29].

One dimensional (1D) simulations were performed using 1D engine simulation program WAVE [30] in order to provide the initial and boundary conditions for the 3D CFD simulations, as shown in Table 2. The initial mixture components in the scavenge ports and the components at the inlet boundary of scavenge ports are pure air, i.e. O_2 and N_2. The initial mixture components in the cylinder are pure burned gas, i.e. CO_2, H_2O and N_2. The boundary conditions, as shown in Table 2, were fixed throughout the simulations in this study. The engine speed was fixed at 2000 rpm. The CFD simulations were carried out from 100 ^{0}CA

after top dead center (TDC) to 280 ^{0}CA, which covers the whole period of the scavenging process. The crank angle used in this paper is referenced to TDC.

The ES-ICE software was used to generate the moving mesh for simulations. The arbitrary sliding interface (ASI) was applied between the scavenge ports and the cylinder liner to control the attachment and detachment with the piston movement. The opening and closure of the scavenge ports were determined by the movement of the piston top and the effect of top land was not considered in this study. ASI was also applied to control the connectivity between exhaust domains and cylinder domain with the movement of exhaust valves. The mesh sensitivity study performed in our previous work [28] indicated that the mesh with an average grid size of 1.6 mm was able to reproduce the same results as finer mesh and was adopted in this study.

Table 2. Simulation conditions.

Initial conditions @ 100 ºCA	
Cylinder temperature	1665 K
Cylinder pressure	8.6 bar
Intake temperature	350 K
Intake pressure	2 bar
Exhaust temperature	800 K
Exhaust pressure	1.06 bar
Boundary conditions	
Intake temperature	350 K
Intake pressure	2 bar
Exhaust temperature	800 K
Exhaust pressure	1.06 bar
Piston head temperature	440 K
Cylinder top temperature	522 K
Cylinder liner temperature	384 K

4. Results and discussions

4.1 Effect of the axis inclination angle (AIA) on the scavenging process

In this section, the axis inclination angle (AIA) was varied from 60^0 to 90^0 to investigate its impact on the in-cylinder flow motion and scavenging process. The swirl orientation angle (SOA) was fixed at the baseline value (20^0). The exhaust valve duration (ED) was fixed at 126 ^{0}CA and the exhaust valve opening (EVO) timing is fixed at 117 ^{0}CA. The scavenge port opening duration (SD) was fixed at 116 ^{0}CA with the corresponding scavenge port opening (SPO) timing at 122^0 CA. Fig. 2 shows the normalized scavenge port opening area (SA') profile and normalized exhaust valve lift (EL') profile used in this section. The scavenge port opening area is defined as the total cross section area of scavenge ports opened by the piston top.

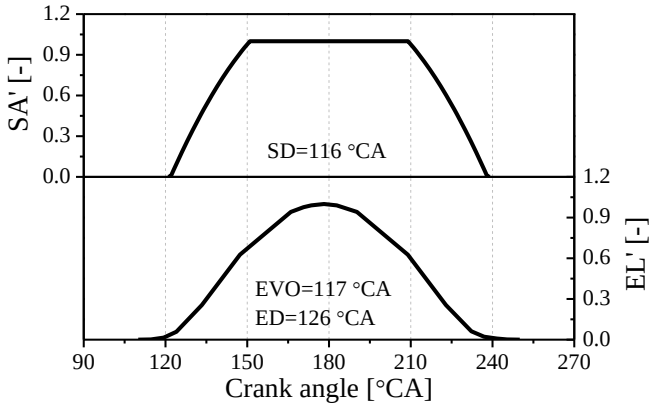

Fig. 2. Schematic diagram of the normalized exhaust valve lift profiles (EL') and scavenge port opening area (SA') profiles

Fig. 3 shows the in-cylinder flow field and residual gas fraction (RGF) distribution during the scavenging process with different AIAs. In the case with AIA of 60^0, the intake flow jets move upward to the cylinder head. With the AIA increased to 90^0, the intake flow jets travel along the piston top and displace the residual gas in the center of cylinder, leading to much lower RGF in the piston bowl.

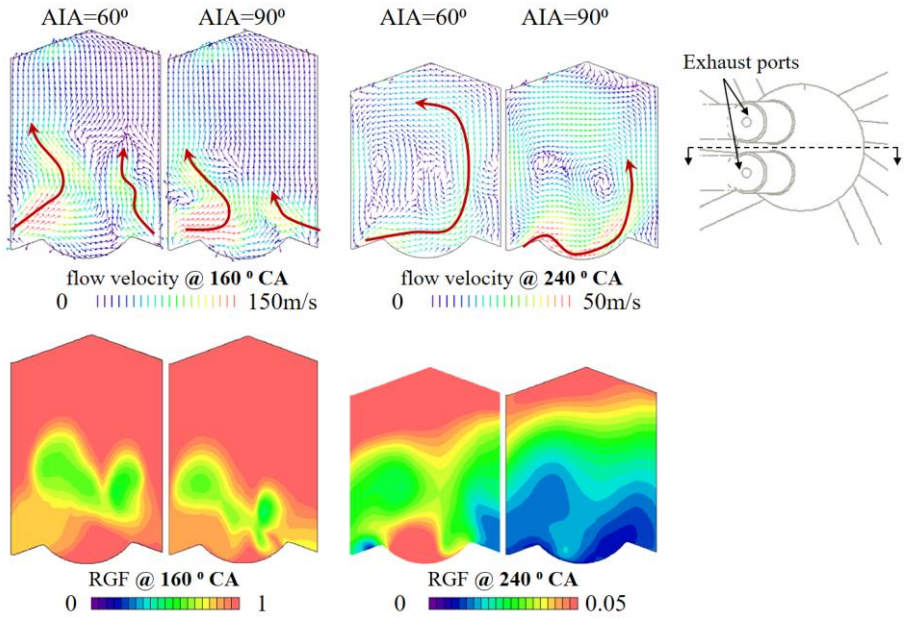

Fig. 3 Comparison of the in-cylinder flow field and residual gas fraction (RGF) distribution at 160 ^{0}CA and 240 ^{0}CA for AIA=60^0 and 90^0.

In order to quantify the overall flow motions, the swirl ratio (SR) is defined by the following equation [31]:

$$SR(\theta) = \frac{\sum_i^m v_i(\theta) r_i(\theta) V_i(\theta) \rho_i(\theta)}{\frac{2\pi n}{60} \sum_i^m r_i(\theta)^2 V_i(\theta) \rho_i(\theta)} \quad (1)$$

where n is engine speed [rpm], θ the crank angle, i the cell number, $V_i(\theta)$ the cell volume, $\rho_i(\theta)$ the cell density, $v_i(\theta)$ and $r_i(\theta)$ are the tangential velocity and radius respectively in the cylindrical coordinate with z axis as the swirl axis.

Similarly, the tumble ratio (TR) and cross tumble ratio (CTR) are determined by replacing the swirl axis along with the cylindrical coordinate system in Equation (1) with the tumble/cross tumble axis which is parallel to the y/x axis and crosses the central point between maximum and minimum z value of the cylinder. The definitions of SR, TR and CTR are schematically shown in Fig. 1.

Fig. 4 shows the effect of AIA on the in-cylinder swirl ratio (SR), tumble ratio (TR) and cross tumble ratio (CTR) at 280 ^{0}CA. The SR is very strong and varies between 6 and 7 for different AIA designs. As AIA increases from 60^0 to 68^0, the SR becomes slightly lower because of the enhanced interaction of the intake flow jets and the piston top. Further increase in the AIA to 75^0 and 90^0 leads to stronger intake flow jets and higher SR because of the dominant effect of the increased effective scavenging area. It should be noted that the scavenge port height was kept constant for different AIAs.

Thanks to the current piston top design with a bias ridge and separated distribution of 8 scavenge ports at two opposite sides, the strong clockwise tumble flow motion, as shown by the flow field distribution at 240 °CA in Fig. 3, is produced for each AIA design. The increase in AIA leads to enhanced interactions between intake flow jets and piston top, which promotes the formation of the tumble flow and cross tumble flow motion. Further increase of AIA to 90^0 leads to stronger horizontal flow into the center of the cylinder but weaker organized vertical flow motion in the outer region. This is not conductive to form the tumble and cross tumble motion and leads to lower TR and much reduced CTR at AIA of 90^0, as shown in Fig. 4.

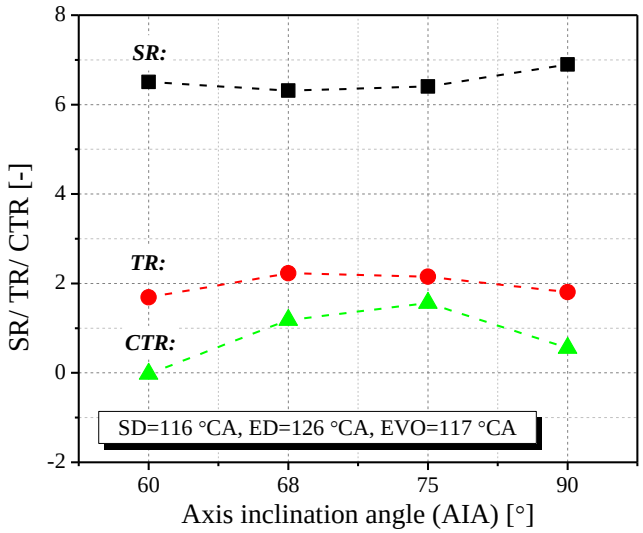

Fig. 4. Effect of AIA on in-cylinder flow motions (SD=116 ^{0}CA, ED=126 ^{0}CA, EVO=117 ^{0}CA).

In order to quantify the scavenging performance, four scavenge parameters, i.e. delivery ratio (DR), trapping efficiency (TE), scavenging efficiency (SE) and charging efficiency (CE), are defined as following:

$$\mathrm{DR} = \frac{\text{delivered fresh charge mass}}{\text{reference mass}} \tag{2}$$

$$\mathrm{TE} = \frac{\text{mass of delivered fresh charge retained in the cylinder}}{\text{total mass of delivered fresh charge}} = \frac{\mathrm{CE}}{\mathrm{DR}} \tag{3}$$

$$\mathrm{SE} = \frac{\text{mass of delivered fresh charge retained in the cylinder}}{\text{total mass of trapped cylinder charge}} \tag{4}$$

$$\mathrm{CE} = \frac{\text{mass of delivered fresh charge retained in the cylinder}}{\text{reference mass}} \tag{5}$$

The reference mass in above equations is calculated by the displaced volume multiplied by the ambient air density.

As the bigger AIA leads to larger effective scavenging area, the DR gradually increases with AIA, as shown in Fig. 5. In order to understand the short-circuiting phenomenon, the residual gas fraction (RGF) profiles in the cylinder (x-axis) and exhaust ports (y-axis) are compared in Fig. 6 for different AIA designs. The scavenge process begins from top right corner where RGF in the cylinder and exhaust ports is 1. Then the RGF in the cylinder gradually decreases with the scavenging process because of the introduction of the fresh intake charge. The decrease of RGF in the exhaust ports indicates the occurrence of short-circuiting phenomenon. As shown in Fig. 6, an AIA of 60 ^{0} leads to earlier and stronger short-circuiting as the intake flow jets from scavenge ports go directly towards the exhaust valves, as shown in Fig. 3. The larger AIA weakens the short-circuiting and meanwhile increases CE. Although the bigger AIA leads to larger DR and CE, it also enhances the mixing between fresh intake charge and residual gas in the cylinder center, which increases the residual gas mass retained in the

cylinder and limits the increase of SE to some extent. Therefore, the SE remains almost constant as AIA increases. It should be noted that the total mass of in-cylinder charge at the end of scavenging gradually increases from 843 to 869 mg as AIA increases from 60° to 90° because of the reduced short-circuiting, which in turn explains the higher CE with almost constant SE.

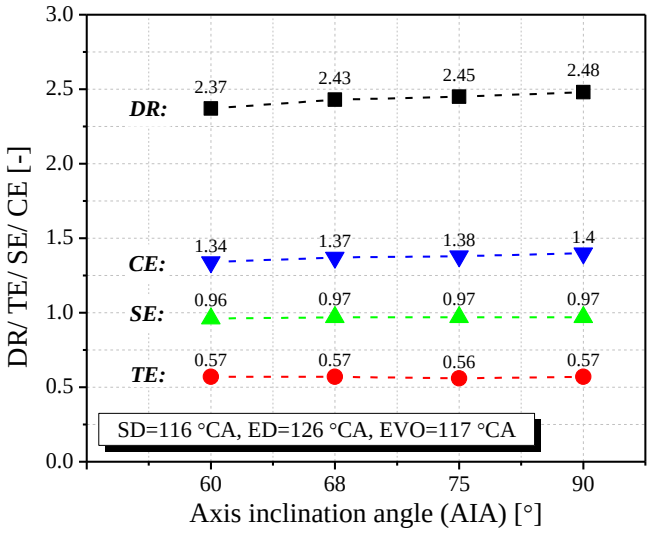

Fig. 5. Effect of AIA on DR, TE, SE and CE (SD=116 ^{0}CA, ED=126 ^{0}CA, EVO=117 ^{0}CA).

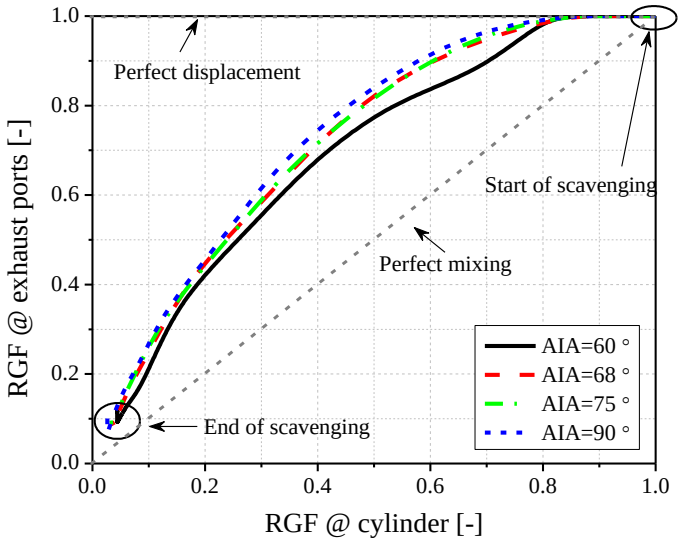

Fig. 6. Comparison of RGF profiles in the cylinder and exhaust ports for different AIAs.

4.2 Effect of the swirl orientation angle (SOA) on the scavenging process

In this section, the effect of SOA on controlling in-cylinder flow motion and scavenging process is investigated with the AIA of 90^0. As shown in Fig. 7, in the case of SOA=0^0, the scavenge flow jets from the eight scavenging ports collide in the cylinder centre and form the strong vertical flow motion from the piston top to the cylinder head. As a result, the fresh charge would be directly pushed to the exhaust ports, as indicated by the flow field and RGF distributions at 180 ^{0}CA. This results in earlier and stronger short-circuiting after the opening of scavenge ports but at the expense of weaker later scavenging, which leaves the central region with the highest RGF concentrate at 240 ^{0}CA.

In comparison, the flow structure is dominated by strong swirl flow motion for SOA of 31.5^0. The strong swirl flow motion drives the fresh intake charge to the cylinder head along the cylinder wall and results in poor scavenging at the cylinder center, as shown by the RGF distribution at 180 ^{0}CA. With the scavenging proceeding, the fresh charge gradually penetrates into the cylinder center and push out the residual gas. The spinning fresh charge behaves like a virtual piston and pushes out the residual gas so that most residual gas ends up at the top of cylinder towards the end of scavenging.

At 240 ^{0}CA, it is noted that a strong tumble flow motion can be observed in the vertical plane for SOA of 0 and 31.5^0. This strong tumble motion is mainly formed by the stronger intake charge motion from the scavenge ports at exhaust sides because of the slightly lower edge of piston top at exhaust sides in order to match the asymmetric cylinder head. This can be verified by the flow motion from exhaust sides to the other side at the horizontal plane for SOA of 0^0. This intake flow motion helps to scavenge the residual gas on the piston top for SOA of 0^0, but shows limited improvement for a large SOA of 31.5^0.

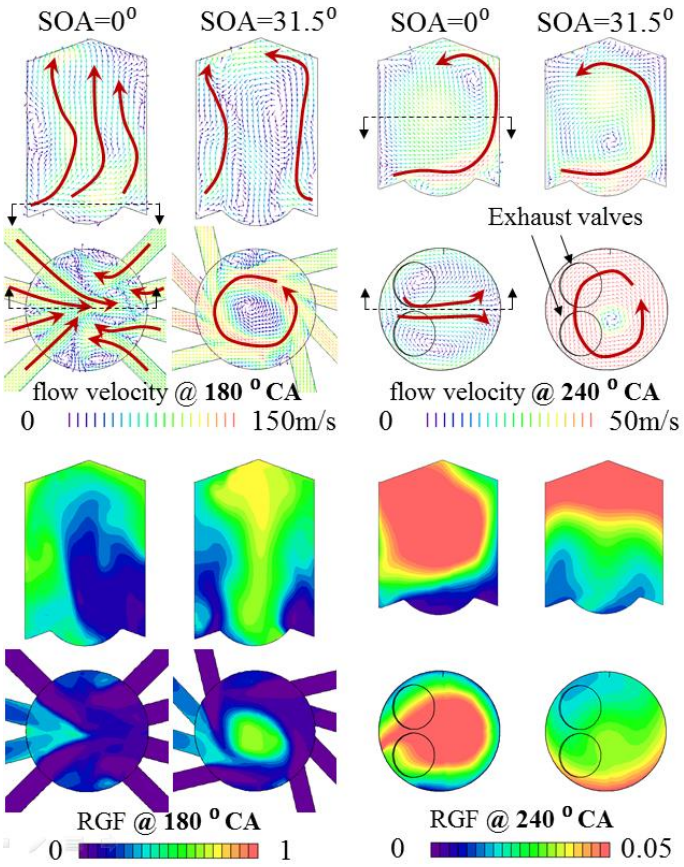

Fig. 7. Comparison of the in-cylinder flow field and residual gas fraction (RGF) distribution at 180 ^{0}CA and 240 ^{0}CA for SOA=0^0 and 31.5^0.

Fig. 8 quantitatively shows the effect of SOA on the SR, TR and CTR at 280 ^{0}CA. As SOA increases, the swirl flow motion would be significantly enhanced because of the increased flow velocity at the outer region of the cylinder. This contributes to the strong positive correlation between SR and SOA as shown in the figure. The enhanced swirl flow motion also helps to form the vertical flow motion thanks to the guidance of the piston shape. The TR and CTR are gradually enhanced with increasing SOA.

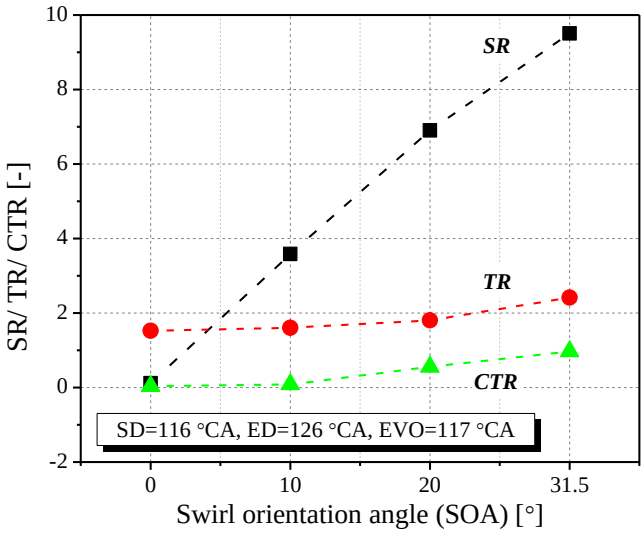

Fig. 8. Effect of SOA on in-cylinder swirl ratio (SR), tumble ratio (TR) and cross tumble ratio (CTR) at 280 ^{0}CA (SPO=122 ^{0}CA, ED=126 ^{0}CA, EVO=117 ^{0}CA).

Fig. 9 shows the effect of SOA on the scavenging performances. It should be noted that the segment of each scavenge port on the cylinder circumference was kept constant for different SOAs. The delivery ratio (DR) is gradually reduced with SOA because of the reduced effective scavenging area. Although the flow motion is gradually enhanced with increasing SOA, the scavenge efficiency (SE) decreased slightly due to the residual gas trapped near the cylinder head as shown in Fig. 7. The smaller SOA leads to non-organized in-cylinder flow motion and earlier charge short-circuiting, as indicated by the RGF distribution in Fig. 7. This in turn leads to lower CE although the DR is higher for small SOA. This can also be verified from the RGF profiles in the cylinder and exhaust ports in Fig. 10. As SOA is increased to 10^0 and 20^0, the moderate swirl flow motion of the intake charge delays the short-circuiting. A further increase of SOA to 31.5^0 leads to the lower DR and early short-circuiting near the cylinder wall with insufficient scavenging in the cylinder center, as shown in Fig. 7, which explains the lower CE and SE. The TE increases slightly with SOA because of the relatively lower DR.

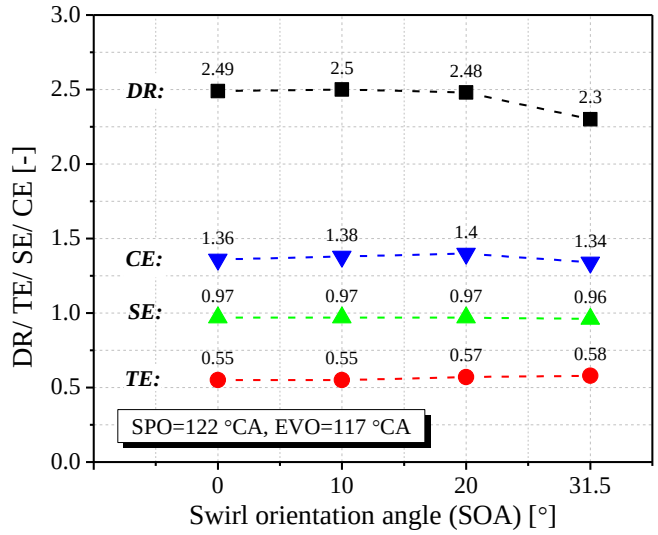

Fig. 9. Effect of SOA on DR, TE, SE and CE (SD=116 ^{0}CA, ED=126 ^{0}CA, EVO=117 ^{0}CA).

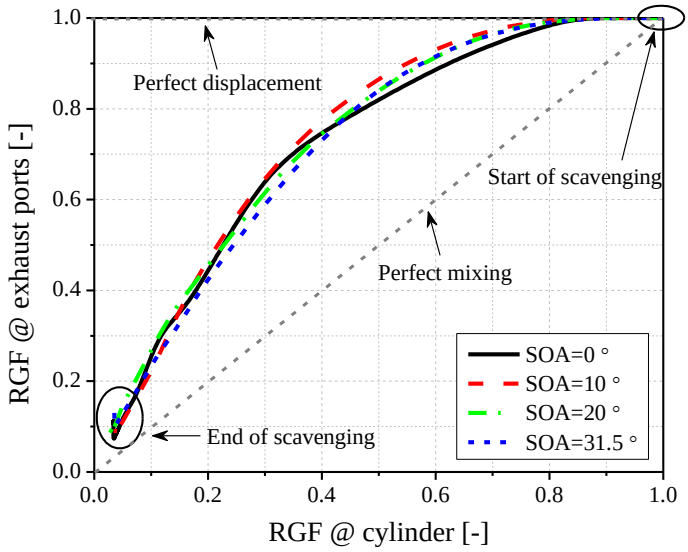

Fig. 10. Comparison of RGF profiles in the cylinder and exhaust ports for different SOAs.

4.3 Effects of scavenge port/exhaust valve opening durations and timings

In this section, the simulations with different combinations of scavenge port opening duration (SD), exhaust valve opening duration (ED) and exhaust valve opening (EVO) timing were performed to understand their impacts on the in-cylinder flow motions and scavenging performances in the BUSDIG engine. The normalized scavenge port opening area (SA') profiles and normalized exhaust valve lift (EL') profiles are shown in Fig. 11 to demonstrate the scavenge port/exhaust valve opening profiles used in this section. The scavenge port

opening (SPO) timing, determined by the upper edge of the scavenge ports, is varied from 116 ^{0}CA to 128 ^{0}CA with SD decreasing from 128 ^{0}CA to 104 ^{0}CA. The EVO timing is changed from 107 to 141 ^{0}CA for the short ED of 98 ^{0}CA and from 107 to 127 ^{0}CA for the long ED of 126 ^{0}CA. The optimal scavenge port angles with AIA of 90^0 and SOA of 20^0 were adopted.

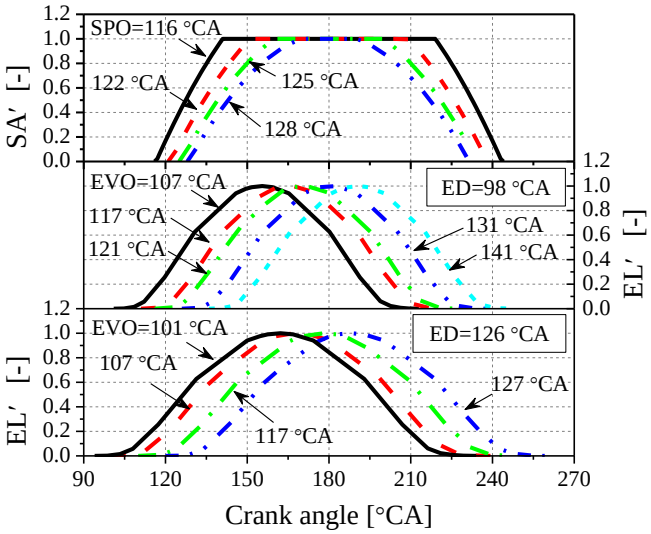

Fig. 11. Normalized scavenge port opening area (SA') profiles and exhaust valve lift (EL') profiles.

In order to facilitate the understanding of the scavenging process in BUSDIG engine, four distinct scavenging periods are proposed and analysed in this study based on the mass flow rate and RGF profiles at the outlets of scavenge ports, as shown in Fig. 12 for a given intake port design and exhaust valve profile. During the first period (I), i.e. the early backflow (EB), the in-cylinder residual gas flows into the scavenge ports immediately after SPO because of the relatively higher pressure in the cylinder. As the in-cylinder pressure decreases, the early backflow slows down. When the in-cylinder pressure drops below the intake pressure, the mixture of residual gas from the early backflow and fresh intake gas starts flowing into the cylinder and scavenges out the in-cylinder residual gas. Because of the involvement of the

mixture of early backflow in the scavenging process, this second period (II) is termed as the backflow scavenging (BS) process. In the third period (III), i.e. main scavenging (MS) process, the pure fresh charge flows into the cylinder pushing out the in-cylinder charge. Under some circumstances, especially for the cases with the scavenge port closing (SPC) timing later than exhaust valve closing (EVC) timing, the in-cylinder mixture would flow back into the scavenge ports because of the increased in-cylinder pressure during the compression stroke. This process is defined as the fourth period (IV) of the post backflow (PB). The durations of these four scavenge periods are defined as d_{EB}, d_{BS}, d_{MS} and d_{PB} respectively.

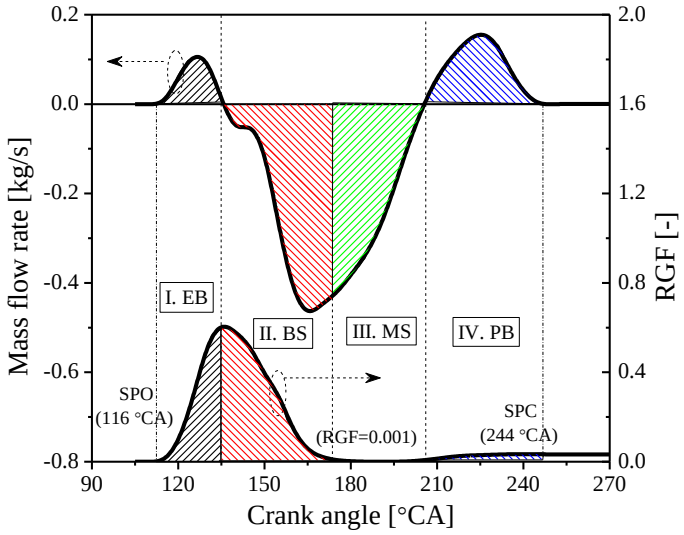

Fig. 12. The total mass flow rate and RGF profile at the outlets of scavenge ports, and the definitions of early backflow (EB), backflow scavenging (BS), main scavenging (MS) and post backflow (PB) periods. (SD=128 ^{0}CA, ED=98 ^{0}CA and EVO=107 ^{0}CA)

The effect of ED and EVO timings on the scavenging process will be discussed in detail for the longest SD of 128 ^{o}CA and shortest SD of 104 ^{o}CA at first. A comprehensive comparison of the results with different SDs, EDs and EVOs will then be made with respect to their impacts on the in-cylinder flow and scavenging performance. Based on these results, the

mechanism of the interactions of scavenge port/exhaust valve opening profiles and their impacts on in-cylinder flow motions and scavenge performances will then be discussed.

4.3.1 Effects of EDs and EVO timings on the scavenging process for the longest SD of 128 ^{0}CA

Fig. 13 compares the total mass flow rate profiles at the outlets of scavenge ports for different EVOs with SD of 128 ^{0}CA and ED of 98 ^{0}CA. The durations for different scavenging periods are given in Table 3. As the delayed EVO timing leads to the shorter blowdown duration, the early backflow duration (d_{EB}) gradually increases and in turn leads to the longer backflow scavenging duration (d_{BS}). However, it is noted that the increases of d_{EB} and d_{BS} become slower after EVO of 117 ^{0}CA because the mass flow rate of the backflow is approaching its peak value, as seen in Fig. 13. The delayed EVO timing also leads to later EVC timing and shortens the post backflow duration (d_{PB}). As a result, the main scavenge duration (d_{MS}) is reduced as the EVO timing is retarded from 107 ^{0}CA to 117 ^{0}CA. As the EVO is further retarded, the post backflow duration (d_{PB}) is reduced more significantly than the early backflow duration (d_{EB}) and backflow scavenging duration (d_{BS}), leading to increased main scavenging duration (d_{MS}). At the latest EVO timing of 141 ^{o}CA, the post backflow has disappeared completely although EVC (239 ^{o}CA) is still earlier than the scavenge port closing (SPC) timing of 244 ^{o}CA, which indicates that the in-cylinder pressure is kept lower than the scavenge port pressure after EVC because of the gas dynamics effect of the exhaust flow. Thus, in order to maximize the scavenging process, the EVC timing can be adjusted to just avoid the post backflow to utilize this post-charging effect at different engine operating conditions for the fixed SPC.

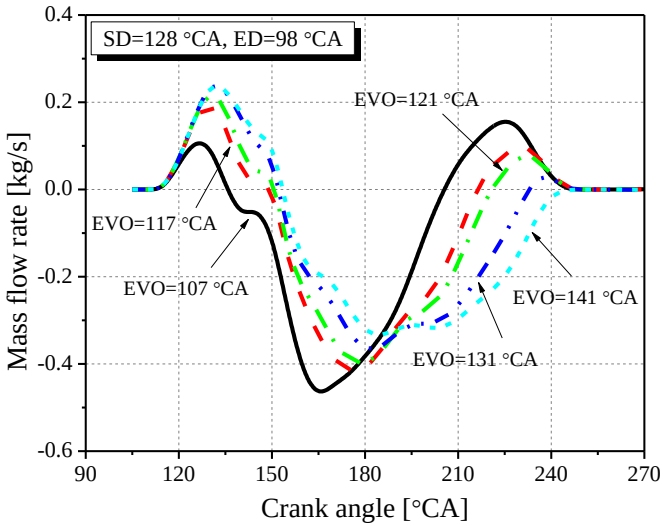

Fig. 13. The total mass flow rate profiles at the outlets of scavenge ports for different EVOs.

(SD=128 ^{0}CA, ED=98 ^{0}CA)

Table 3. Effect of EVO timing on scavenging durations (SD=128 ^{0}CA, ED=98 ^{0}CA).

EVO [^{0}CA]	d_{EB} [^{0}CA]	d_{BS} [^{0}CA]	d_{MS} [^{0}CA]	d_{PB} [^{0}CA]
107	19.68	36.49	33.23	38.6
117	34.43	38.37	27.51	27.69
121	35.3	41.49	27.79	23.42
131	36.24	47.34	33.2	11.21
141	37.41	50.6	39.99	0

Fig. 14 shows the impact of EVO timing on SR, TR and CTR at 280 ^{0}CA. As shown in Fig. 13, the delayed EVO timing leads to delayed main scavenging phasing which is defined by the crank angle with peak mass flow rate during the main scavenging period. The delayed scavenging phasing, on the one hand, facilitates the formation of the in-cylinder flow motion and enhances the interactions between the intake flow jets and the piston top as the piston rises. This leads to enhanced tumble flow motion thanks to the piston top geometry, as shown

in Fig. 14. The swirl and cross tumble are less sensitive to the EVO and the SR and CTR peak at an intermediate EVO around 121 ^{0}CA.

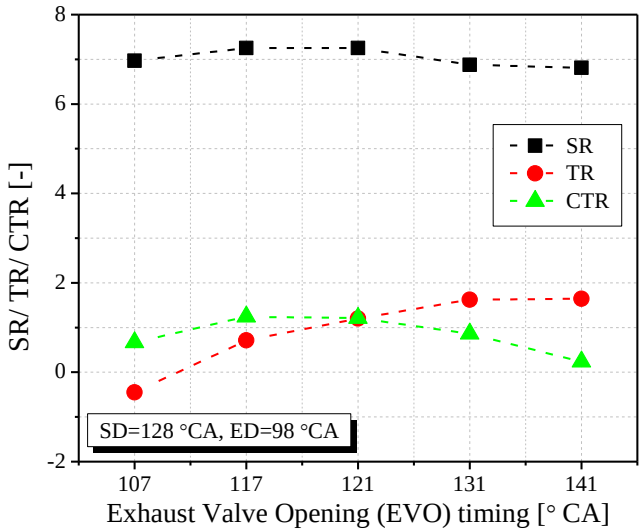

Fig. 14. Effect of EVO timing on the SR, TR and CTR at 280 ^{0}CA (SD=128 ^{0}CA, ED=98 ^{0}CA).

Fig. 15 shows the effect of EVO timing on the scavenging process as measured by DR, TE, SE and CE. The DR reduces slightly at EVO of 117 ^{0}CA and then increases afterwards, following the same trend as the change of the main scavenge duration (d_{MS}) with EVO shown in Table 3. The gradually reduced post backflow duration (d_{PB}) with the delayed EVO timing also contributes to the increasing trend of DR. Similarly, the CE also increases with the retarded EVO because of the reduced post backflow with delayed EVO timing, which would trap more charge in the cylinder although the peak mass is lower, as shown in Fig. 16. However, as the whole scavenging phasing is significantly delayed beyond EVO of 131 ^{o}CA, the final mass trapped in the cylinder is lowered slightly because of the increased early backflow and diminished post-charging effect.

The scavenging efficiency (SE) is negatively affected by the increased early backflow duration (d_{EB}) when the EVO is delayed from 107 to 117 ^{0}CA. It then gradually recovers

after 117 ^{0}CA because of the increased main scavenging period. As the trapping efficiency (TE) is calculated by the ratio of charging efficiency (CE) to delivery ratio (DR), it peaks at intermediate EVOs.

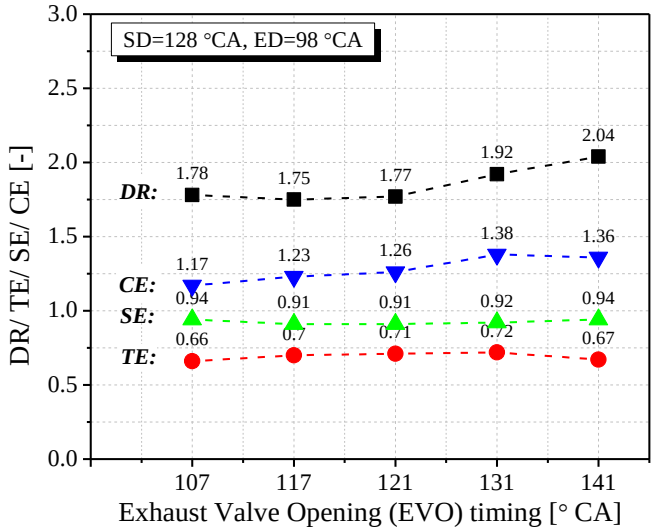

Fig. 15. Effect of EVO timing on DR, TE, SE and CE (SD=128 ^{0}CA, ED=98 ^{0}CA).

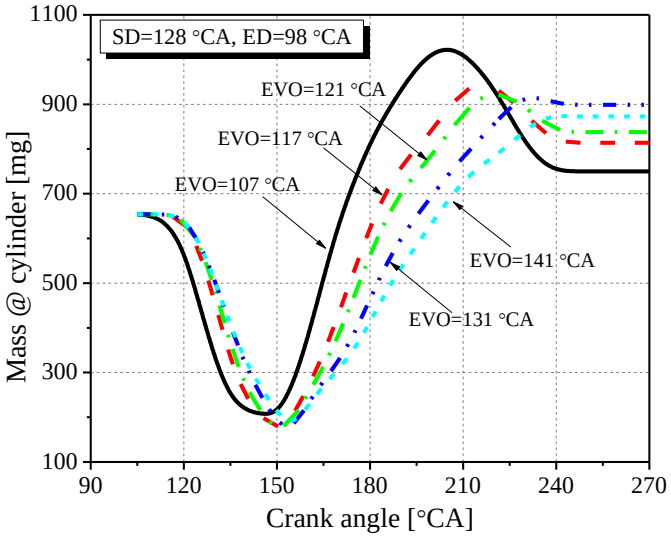

Fig. 16. Cylinder mass evolutions with different EVOs (SD=128 ^{0}CA, ED=98 ^{0}CA).

Fig. 17 shows the total mass flow rate profiles at the outlets of scavenge ports for the long ED of 126 ^{0}CA and SD of 128 ^{0}CA. Table 4 quantitatively compares the durations for different scavenging periods. Overall, the mass flow rate profiles for the longer ED of 126 ^{0}CA show

similar trends to the short ED of 98 ^{0}CA. For the longer ED, the slop of the exhaust valve opening profile is less steep than that of the shorter ED, leading to higher sensitivity of d_{EB} and d_{BS} to the EVO timing. The early backflow duration (d_{EB}) and backflow scavenge duration (d_{BS}) are increased slightly for the longer ED, which can be verified by comparing the scavenging durations for EVOs of 107 ^{0}CA and 117 ^{0}CA in Tables 3 and 4.

As shown in Table 4, when EVO is changed from 101 to 107 ^{0}CA, both d_{EB} and d_{BS} increase but d_{EB} is less sensitive to EVO than the d_{BS} because of the lower exhaust valve lift profile during the backflow scavenging period. As EVO is delayed from 107 to 117 ^{0}CA, the d_{EB} exhibits much significant increase than the d_{BS} because of the higher exhaust valve lift profile during the backflow scavenge period. Further delay of EVO to 127 ^{0}CA leads to little change in d_{EB} but much longer d_{BS}. Both the main scavenging period and post backflow period decrease with EVO delaying. The post backflow is completely avoided with the most retarded EVO.

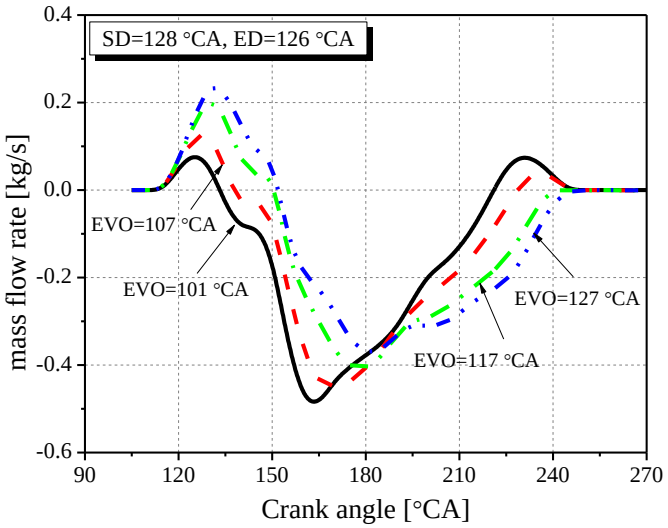

Fig. 17. The total mass flow rate profiles at the outlets of scavenge ports for different EVOs. (SD=128 ^{0}CA, ED=126 ^{0}CA)

Table 4. Effect of EVO on scavenging durations, SD=128 ^{0}CA, ED=126 ^{0}CA.

EVO [^{0}CA]	d_{EB} [^{0}CA]	d_{BS} [^{0}CA]	d_{MS} [^{0}CA]	d_{PB} [^{0}CA]
101	17.12	30.37	57.53	22.98
107	21.71	39.62	51.13	15.54
117	35.14	39.73	48.91	4.22
127	36.05	46.89	45.06	0

Fig. 18 compares the SR, TR and CTR at 280 ^{o}CA for different EVOs with ED of 126 ^{0}CA and SD of 128 ^{0}CA. The delayed and prolonged main scavenging period enhances the in-cylinder flow motion with the retarded EVO, resulting higher tumble and swirl ratios but slightly lower cross tumble flows due to the strong interaction of the scavenge flow jets and piston top.

Compared to the shorter ED of 98^{0}CA, a longer ED of 126 ^{0}CA leads to better DR and SE, as shown in Fig. 19, due to longer main scavenging duration (d_{MS}). However, the significant improvement in CE can only be achieved at early EVOs for the longer ED.

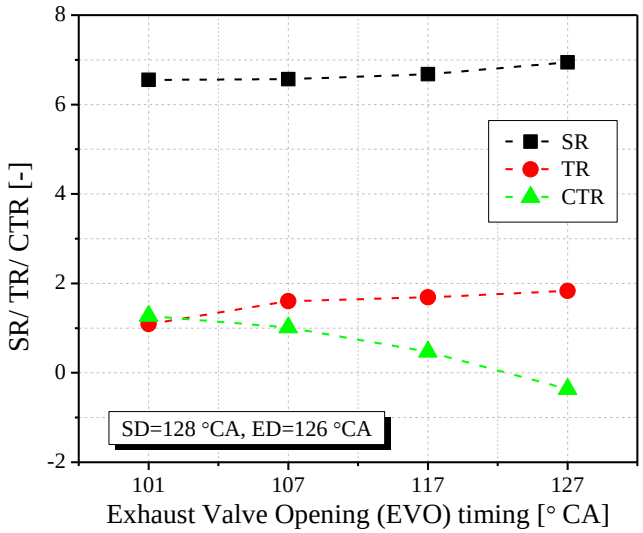

Fig. 18. Effect of EVO on the SR, TR and CTR at 280 ^{0}CA (SD=128 ^{0}CA, ED=126 ^{0}CA).

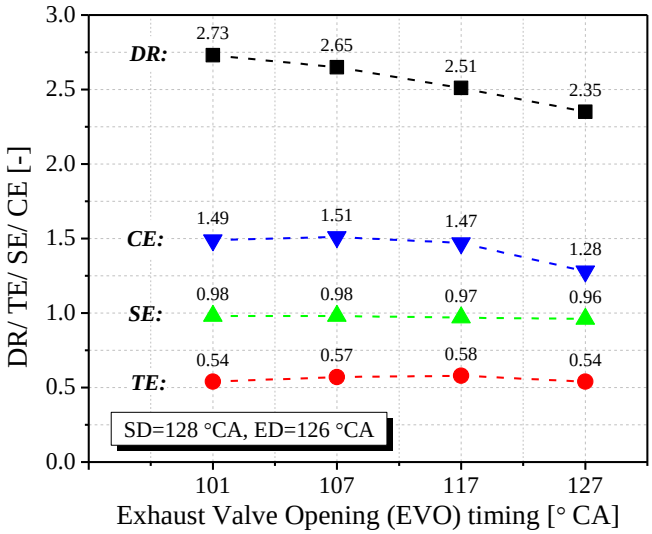

Fig. 19. Effect of EVO on DR, TE, SE and CE (SD=128 ^{0}CA, ED=126 ^{0}CA).

4.3.2 Effects of EDs and EVO timings on the scavenging process for the shortest SD of 104 ^{0}CA

Fig. 20 and 21 show the effect of EVO timing on in-cylinder flow motions and scavenging performances with the shortest SD of 104 ^{0}CA and ED of 98 ^{0}CA. As shown in Fig 20, the swirl ratio is slightly affected by the EVO and it peaks at an intermediate EVO timing. With a shorter SD, the delayed EVO timing produces higher peak TR due to enhanced intake flow. The delayed EVO timing leads to more delayed scavenging phasing with smaller scavenging area during the main scavenging period. Meanwhile, the later EVO timing also produces quicker pressure drop in the cylinder after the bottom dead center (BDC) due to larger valve lifts during the scavenging. This in turn leads to increased pressure difference between the intake scavenge ports and cylinder and produces higher intake velocity. At the closing of the scavenge ports, the formed strong tumble flow motion would be significantly deteriorated and transfer to cross tumble flow motion under the influence of the swirl flow motion. As a result, the CTR is even higher than TR and shows an increasing trend with EVO delaying, as shown in Fig. 20.

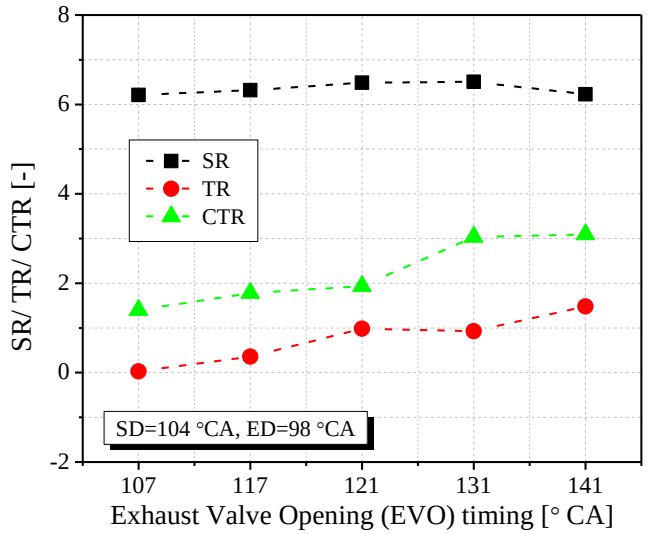

Fig. 20. Effect of EVO timing on the SR, TR and CTR at 280 ^{0}CA (SD=104 ^{0}CA, ED=98 ^{0}CA).

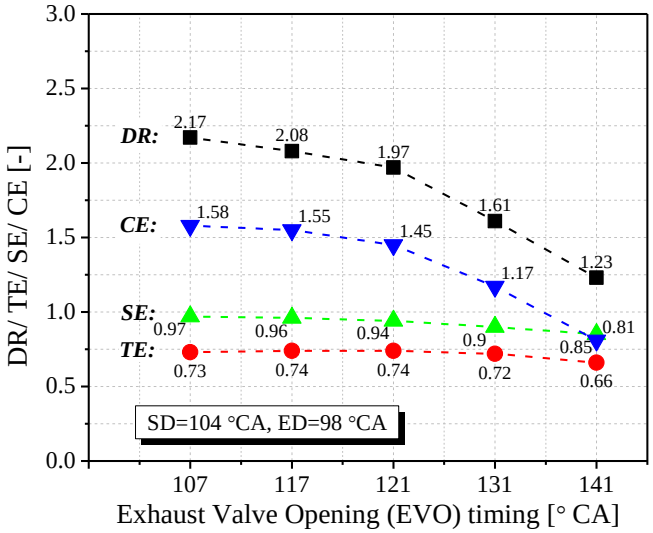

Fig. 21. Effect of EVO timing on DR, TE, SE and CE (SD=104 ^{0}CA, ED=98 ^{0}CA).

Table 5 lists the change of the four scavenging periods as a function of EVO for the shortest SD of 104 ^{0}CA and fixed ED of 98 ^{0}CA. The delayed EVO timing leads to increased d_{EB} and d_{BS} but reduced d_{MS} and d_{PB}. The disappearance of the post backflow period weakens the post-charging effect and contributes to the decrease of d_{MS} at EVOs of 131 and 141 ^{o}CA. As the main scavenging duration (d_{MS}) is shortened by the retarded EVO, the delivery ratio (DR)

and the charging efficiency (CE) are reduced as shown in Fig. 21. The reduction of CE is more significant for the EVO of 127 ^{0}CA when the post backflow disappears. The increased early backflow duration (d_{EB}) with the delayed EVO enhances the pre-mixing between residual gas and fresh air and leads to lower scavenging efficiency (SE).

Table 5. Effect of EVO on scavenging durations (SD=104 ^{0}CA, ED=98 ^{0}CA).

EVO [^{0}CA]	d_{EB} [^{0}CA]	d_{BS} [^{0}CA]	d_{MS} [^{0}CA]	d_{PB} [^{0}CA]
107	9.11	12.35	59.22	23.31
117	18.9	30.95	40.59	13.56
121	21.77	36.93	37.48	7.82
131	33.99	39.83	30.18	0
141	38.74	45.01	20.24	0

As the ED is changed to 126 ^{0}CA, the same effects of the EVO are observed on the durations of each scavenging period, as shown in Table 6. As shown in Fig. 22, with the extended ED of 126 ^{0}CA, the delay in EVO has little impact on SR and causes slight increase in TR and CTR. Similar to the shorter ED, both DR and CE decrease with retarded EVO whilst the SE and TE decrease slightly, as shown in Fig. 23.

Table 6. Effect of EVO timing on the durations of different scavenging periods, SD=104 ^{0}CA, ED=126 ^{0}CA.

EVO [^{0}CA]	d_{EB} [^{0}CA]	d_{BS} [^{0}CA]	d_{MS} [^{0}CA]	d_{PB} [^{0}CA]
101	7.01	3.1	86.18	7.72
107	12.63	18.86	72.51	0
117	20.84	34.71	48.45	0
127	33.56	38.08	32.36	0

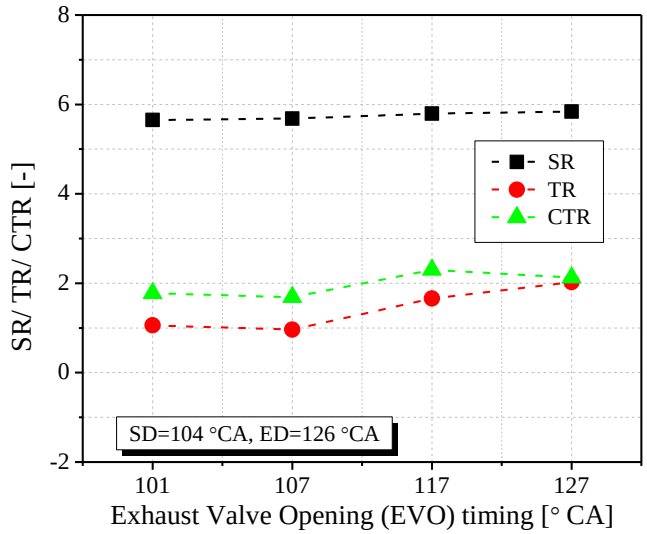

Fig. 22. Effect of EVO timing on the SR, TR and CTR at 280 ^{0}CA (SD=104 ^{0}CA, ED=126 ^{0}CA).

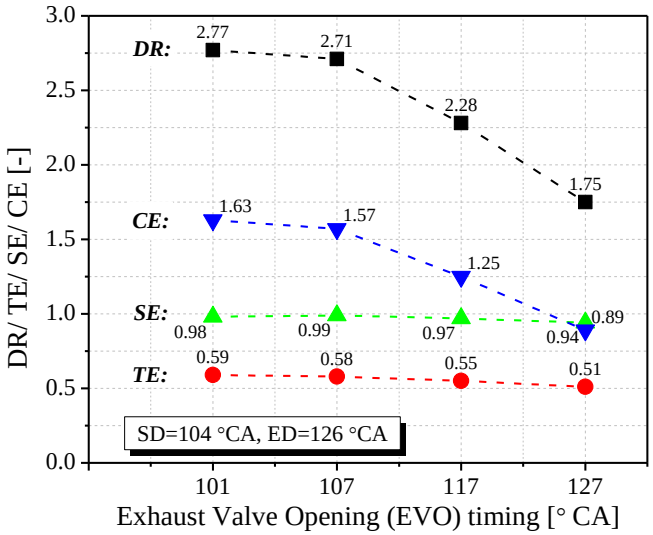

Fig. 23. Effect of EVO timing on DR, TE, SE and CE (SD=104 ^{0}CA, ED=126 ^{0}CA).

4.3.3 Comparison of the effects of SD, ED and EVO timing on the scavenging process

In order to systematically compare the impact of EVO timing on in-cylinder flow motions with all the combinations of SDs and EDs in Fig. 11, the maximum/minimum value and the corresponding changing percentage (δ) of SR, TR and CTR with different EVOs are presented in Table 7. The sensitivity to EVO timing of a parameter is measured by the

percentage of change in the parameter, which is defined as the ratio of the difference between the maximum and minimum value to the maximum value. It can be seen that both the maximum and minimum values of SR decrease with SD. The comparison between EDs indicates that a longer ED leads to a slightly lower SR. The SR is most sensitive to the EVO timing at an intermediate SD around 116 °CA for both EDs.

The maximum TR peaks at an intermediate SD of 110 ^{0}CA for both EDs. A longer ED would increase the TR, especially its minimum value. TR is much more sensitive to the EVO timing, especially for the shorter ED of 98 °CA and a shorter SD. The shortest SD of 104 °CA produces higher maximum CTR for both EDs and the highest maximum CTR of 3.09 with the help of a shorter ED of 98 °CA.

Table 7 Maximum/minimum value and the changing percentage of SR, TR and CTR with different EVOs for different SDs and EDs.

	ED=98 ^{0}CA			ED=126 ^{0}CA		
SD [^{0}CA]	SR_{max} [-]	SR_{min} [-]	δ_{SR} [%]	SR_{max} [-]	SR_{min} [-]	δ_{SR} [%]
128	7.26	6.81	6	6.94	6.55	6
116	7.27	6.57	10	6.9	6.3	9
110	6.96	6.26	10	6.26	6.09	3
104	6.5	6.21	4	5.84	5.65	3
SD [^{0}CA]	TR_{max} [-]	TR_{min} [-]	δ_{TR} [%]	TR_{max} [-]	TR_{min} [-]	δ_{TR} [%]
128	1.64	0.45	73	1.83	1.09	40
116	1.62	0.22	86	2.26	1.22	46
110	2.31	0.02	99	2.42	1.03	57
104	1.48	0.03	98	2.02	0.96	52
SD [^{0}CA]	CTR_{max} [-]	CTR_{min} [-]	δ_{CTR} [%]	CTR_{max} [-]	CTR_{min} [-]	δ_{CTR} [%]
128	1.24	0.24	81	1.27	0.36	72
116	0.88	0.61	31	0.6	0.13	78
110	1.79	1.06	41	1.03	0.21	80
104	3.09	1.4	55	2.3	1.69	27

Shown in Table 8 are the maximum/minimum value and the corresponding percentage of change in each scavenge parameter with EVOs. For the shorter ED of 98 °CA, the maximum DR and CE show an increasing trend with shorter SD. TE and SE also increase slightly with a shorter SD. As the ED increases to 126 ^{0}CA, DR and CE are significantly improved. The SE is also slightly improved but TE is deteriorated. The maximum DR and CE peak at an intermediate SD around 110 ^{0}CA.

The sensitivity of each scavenging parameter shows an increasing trend with a shorter SD. Overall, a longer ED shows better scavenging performances and lower sensitivity to EVO timing. An intermediate SD around 110 ^{0}CA can produce the optimal scavenge performance with the highest maximum DR, SE and CE. A shorter ED produces a higher trapping efficiency, and the scavenging performance can be further improved with a reduced SD.

Table 8 Maximum/minimum value and the changing percentage of each scavenge parameter with different EVOs for different combinations of SD and ED.

	ED=98 ^{0}CA			ED=126 ^{0}CA		
SD [^{0}CA]	DR_{max} [-]	DR_{min} [-]	δ_{DR} [%]	DR_{max} [-]	DR_{min} [-]	δ_{DR} [%]
128	2.04	1.75	14	2.73	2.35	14
116	2.04	1.69	17	2.87	2.09	27
110	2.14	1.46	32	2.87	1.94	32
104	2.17	1.23	43	2.77	1.75	37
SD [^{0}CA]	TE_{max} [-]	TE_{min} [-]	δ_{TE} [%]	TE_{max} [-]	TE_{min} [-]	δ_{TE} [%]
128	0.72	0.66	3	0.58	0.54	2
116	0.73	0.68	5	0.57	0.53	3
110	0.73	0.67	8	0.57	0.51	4
104	0.74	0.66	12	0.59	0.51	4
SD [^{0}CA]	SE_{max} [-]	SE_{min} [-]	δ_{SE} [%]	SE_{max} [-]	SE_{min} [-]	δ_{SE} [%]
128	0.94	0.91	15	0.98	0.96	15
116	0.97	0.92	20	0.99	0.96	32
110	0.97	0.89	36	0.99	0.95	39
104	0.97	0.85	49	0.98	0.94	45
SD [^{0}CA]	CE_{max} [-]	CE_{min} [-]	δ_{CE} [%]	CE_{max} [-]	CE_{min} [-]	δ_{CE} [%]

128	1.38	1.17	8	1.51	1.28	7
116	1.42	1.14	7	1.62	1.1	7
110	1.52	0.98	8	1.64	1	11
104	1.58	0.81	11	1.63	0.89	14

4.3.4 Mechanism of the effect of scavenge port/exhaust valve opening profiles on the scavenging process

In this section, the scavenging process is reviewed at first based on the results shown in the previous sections and the correlations between the key parameters are analyzed. A comprehensive diagram is then drawn to illustrate the mechanism of effect of scavenge port/exhaust valve opening profiles on scavenging process in BUSDIG engine.

A longer SD or delayed EVO timing lead to increased early backflow duration (d_{EB}) due to shorter blow-down duration. The increase of d_{EB} is gradually slowed down due to the limit of the maximum early backflow rate. The effective scavenging flow area of the scavenge ports and the exhaust valve lift profile during the early backflow period affect the in-cylinder pressure and shows impact on d_{EB}. Therefore, the d_{EB} is slightly longer with a longer ED or shorter SD due to the lower slop of the opening profile, and also become more sensitive to EVO timing.

A longer early backflow period usually leads to a longer subsequent backflow scavenge duration (d_{BS}). But in some cases where the increase of d_{EB} is even longer than the increase of EVO timing, the increase of d_{BS} will be slightly weakened due to the higher exhaust valve lift during the backflow scavenging period. Or, in some other cases where the increase of d_{EB} is significantly shorter than the increase of EVO timing, the increase of d_{BS} will be significantly enhanced compared to the increase of d_{EB} due to smaller exhaust valve lift profile during the backflow scavenging period.

The reduction of SD or delaying of EVO monotonously shortens the post backflow duration (d_{PB}). However, with the disappearance of the post backflow, further reduction of SD or

delayed EVO timing would directly reduce the main scavenging duration d_{MS} due to diminished post-charging effect.

The variations of above three scavenge periods, i.e. d_{EB}, d_{BS} and d_{PB}, would finally determine the value of d_{MS}. As the EVO is delayed, d_{MS} shows initially a decreasing trend at the first stage due to significant increase of d_{EB} and d_{BS}. During the second stage, as the increase of d_{EB} slows down due to the limit of the maximum flow rate of early backflow, d_{MS} increases thanks to the much smaller d_{PB}. In the third stage, with the disappearance of the post backflow period, further delay of EVO would lead to the decrease of d_{MS}. It should be noted that the second stage is absent for some cases in which d_{EB} and d_{BS} are very sensitive to EVO timing.

Similarly, the effect of SD on the scavenging process can also be explained. For an early EVO timing (e.g. 107 ^{0}CA with ED of 98 ^{0}CA), the reduction of SD shortens d_{EB} due to the longer blow-down duration, leading to increased d_{MS}. However, for a later EVO timing (e.g. 141 ^{0}CA with ED of 98 ^{0}CA), the reduction of SD leads to early closing of scavenge ports and reduced post-charging effect, which directly reduces the d_{MS}.

The sensitivities of early backflow duration (d_{EB}), backflow scavenge duration (d_{BS}) and post backflow duration (d_{PB}) are mainly controlled by the relationship between the opening profiles of scavenge ports and exhaust valves. The combined sensitivities of d_{EB}, d_{BS} and d_{PB} finally determine the variation of d_{MS} for different combinations of SD, ED and EVO. In order to characterise their impacts on controlling the scavenging process in BUSDIG engine, three parameters, the difference between the opening timings of scavenge ports and exhaust valves (Δ_{open}), the difference between the closing timings of scavenge ports and exhaust valves (Δ_{close}) and the overlap between the opening profiles of scavenge ports and exhaust valves ($\Delta_{overlap}$) are defined as follows and shown in Fig. 24,

$$\Delta_{open} = \text{SPO-EVO} \tag{6}$$

Δ_{close} =SPC-EVC (7)

$\Delta_{overlap}$ =Min (SPC,EVC)-Max(SPO, EVO) (8)

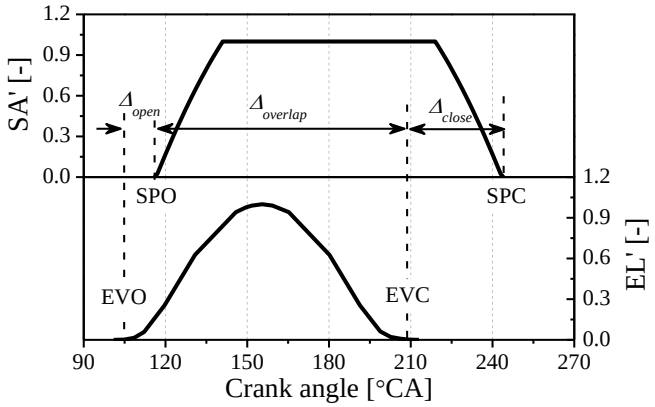

Fig. 24. Definitions of Δ_{open}, Δ_{close} and $\Delta_{overlap}$.

As shown in Fig. 25, d_{EB} gradually decreases with increasing Δ_{open}, characterised with two linear correlation regions. In the case of the negative values of Δ_{open}, indicating earlier SPO timing compared to EVO timing, d_{EB} is relatively longer but shows lower sensitivity to Δ_{open}. In the cases of positive values of Δ_{open}, indicating a blow-down period before the opening of scavenge ports, d_{EB} shows higher sensitivity to Δ_{open} and decreases rapidly with increasing Δ_{open}. The strong positive correlation between d_{EB} and d_{BS} is shown in Fig. 26, and the two distinct regions of the correlations can still be observed. Overall, the d_{BS} increases with d_{EB}.

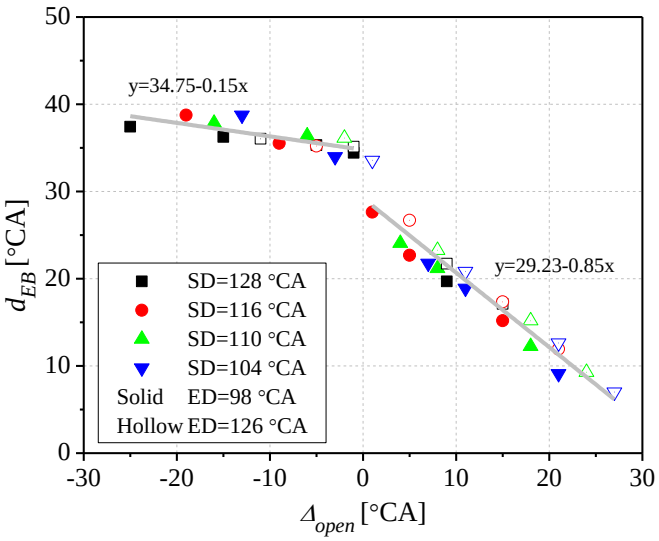

Fig. 25. Correlation of d_{EB} with Δ_{open}.

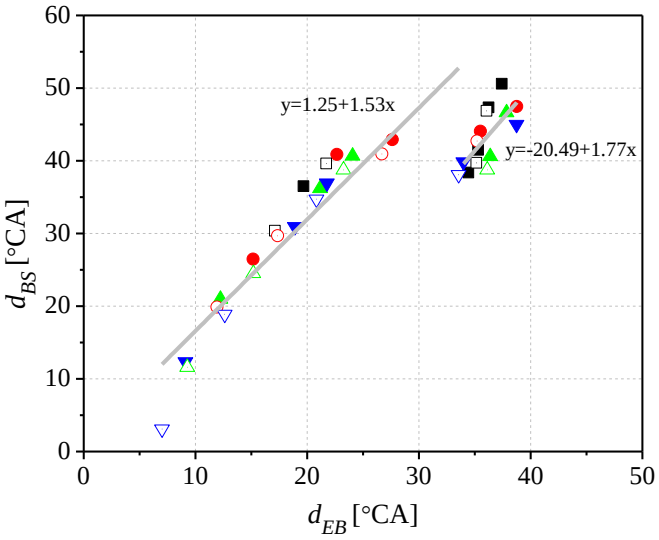

Fig. 26. Correlation of d_{BS} with d_{EB}.

Fig. 27 shows the strong positive correlation between d_{PB} and Δ_{close}. A longer ED leads to an earlier increase of d_{PB} with Δ_{close} because of lower slope of the exhaust valve lift profile with the fixed peak valve lift. For the short ED of 98 °CA, it is noted that the post backflow occurs after Δ_{close} of around 10 °CA instead of 0 °CA, which clearly demonstrates the existence of post-charging effect that the intake charge would still flow into the cylinder after the closing of exhaust valves due to relatively higher intake pressure than the cylinder pressure.

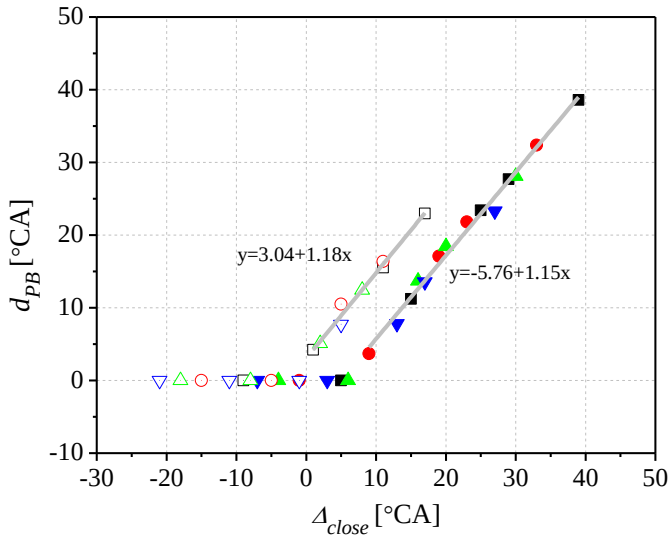

Fig. 27. Correlation of d_{PB} with Δ_{close}.

Fig. 28 shows the complex relationship between d_{MS} and $\Delta_{overlap}$. The square and round symbols indicate the cases with EDs of 98 and 126 °CA respectively. As the post backflow would directly affect the main scavenging period, the solid symbols indicate the cases with post backflow period while hollow symbols indicate cases without post backflow period. In addition, the main scavenging durations of those cases with $\Delta_{overlap}$ equal to SD or ED would be more affected by other factors instead of the overlap ($\Delta_{overlap}$) itself, and those cases are marked as the blue symbols and neglected for the correlation.

For those cases with the post backflow period (solid symbols), the increase in $\Delta_{overlap}$ indicates an earlier SPO timing as well as longer early backflow and backflow scavenging periods, leading to negative correlation of d_{MS} with $\Delta_{overlap}$, as shown in Fig. 28. Therefore, in order to achieve a longer main scavenge duration (d_{MS}), $\Delta_{overlap}$ should be reduced by adjusting the SD and exhaust valve lift profile. The adoption of a long ED can further increase d_{MS}. For those cases without the post backflow (hollow symbols), the increase in $\Delta_{overlap}$ would prolong the d_{MS}, as indicated by the correlation curve (grey) in Fig. 28.

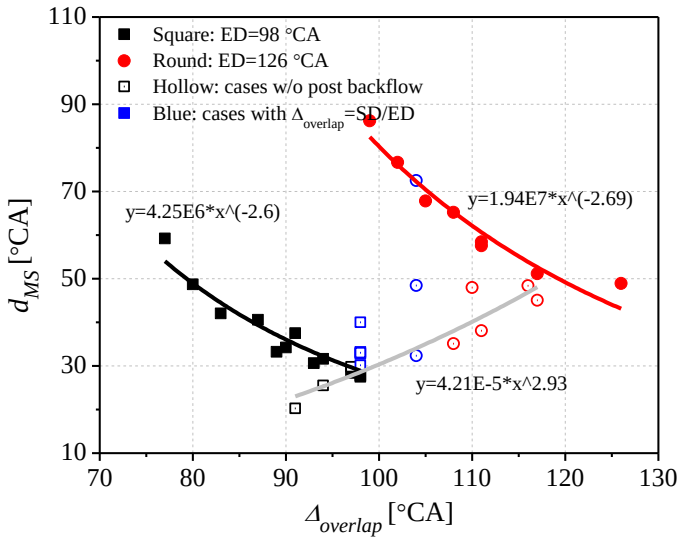

Fig. 28. Correlation of d_{MS} with $\Delta_{overlap}$.

The scavenging process directly controls the in-cylinder flow motions and scavenging performances. Although the main scavenging period directly drives the scavenging process in the cylinder, there is no strong correlation between d_{MS} and the flow motions. In comparison, the SR and TR show good correlations with Δ_{close}, as shown in Fig. 29. A larger Δ_{close} leads to higher SR but lower TR. The increase in Δ_{close} leads to more significant post backflow, indicating more in-cylinder gas entering the scavenging ports on the cylinder wall instead of the exhaust ports on the one side of the cylinder top. This would then slow the decay of SR but weaken the tumble flow motion. The CTR is affected by the evolutions of both SR and TR, showing poor correlation with Δ_{close}.

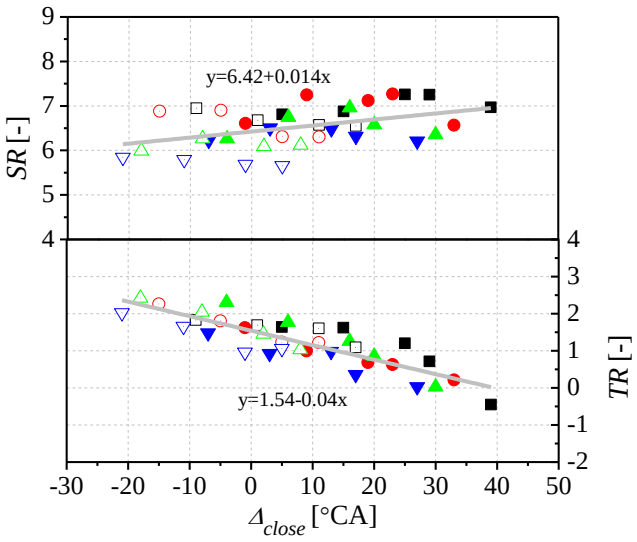

Fig. 29. Correlation of SR and TR with Δ_{close}.

Fig. 30 shows that there are strong positive correlations of SE and CE with DR. The correlation between DR and SE is insensitive to the exhaust valve opening duration (ED) and a larger DR can lead to higher SE. While the correlation between CE and DR is sensitive to the ED. A shorter ED is preferred to achieve a higher CE with same DR.

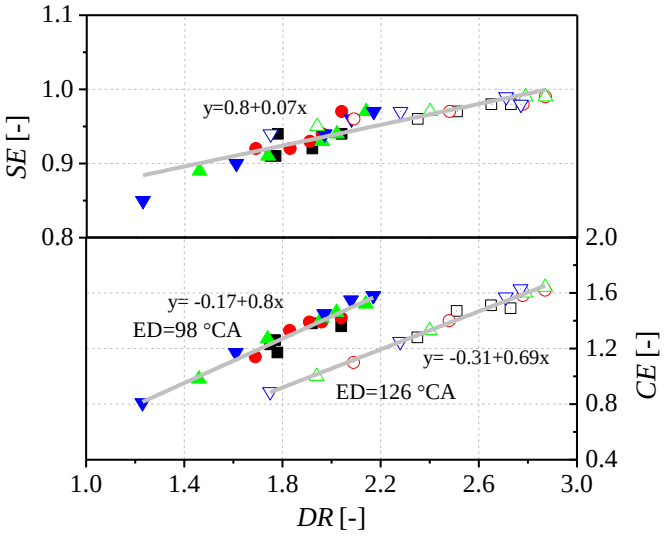

Fig. 30. Correlation of SE and CE with DR.

The correlation between CE and SE is slightly sensitive to ED, as shown in Fig. 31. As a higher SE indicates less fraction of residual gas in the cylinder, the CE shows positive

correlation with SE. Compared to the long ED, a shorter ED leads to stronger post-charging effect and higher in-cylinder total mass, leading to higher CE with the same SE.

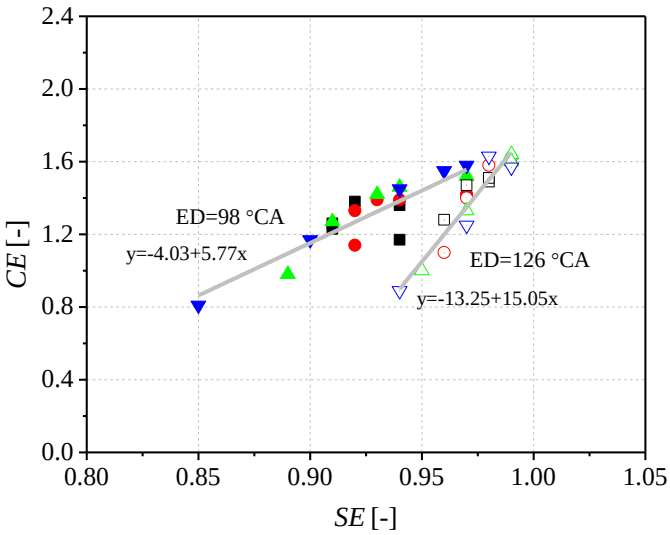

Fig. 31. Correlation of CE with SE.

As the most important scavenging period, the main scavenge duration (d_{MS}) shows strong correlations with DR, SE and CE, as shown in Fig. 32. Overall, DR, SE and CE increase with d_{MS}, while the increasing rates become slower with d_{MS} over 60 °CA.

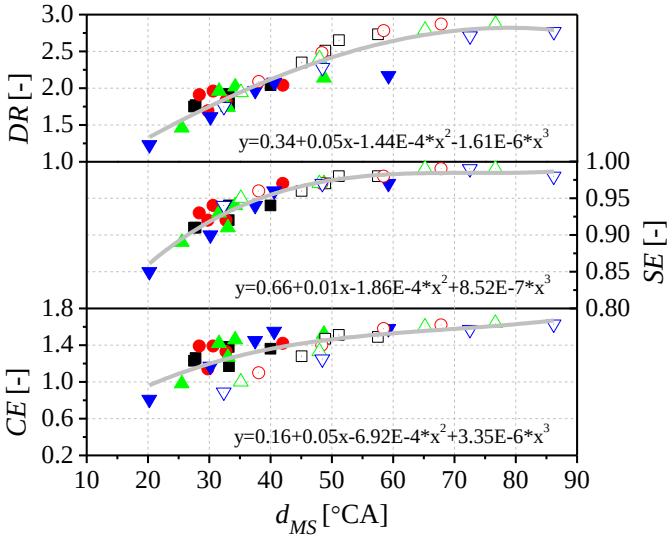

Fig. 32. Correlation of DR, SE and CE with d_{MS}.

Fig. 33 and 34 shows the correlations of SE with d_{EB} and Δ_{open}. The longer early backflow period, usually caused by a smaller Δ_{open}, leads to strong pre-mixing between residual gas and fresh charge and finally reduces the scavenging efficiency (SE). Therefore, a larger Δ_{open} is preferred to reduce the early backflow period and increase SE. However, an improved DR is always helpful to improve the SE, as indicated in Fig. 30.

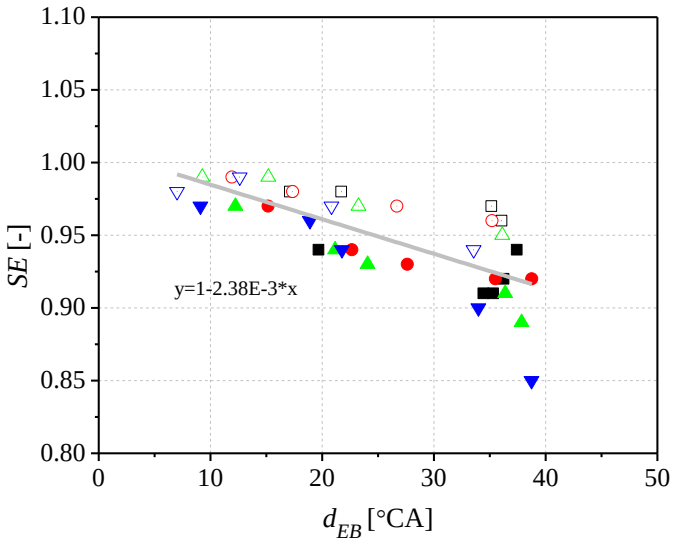

Fig. 33. Correlation of SE with d_{EB}.

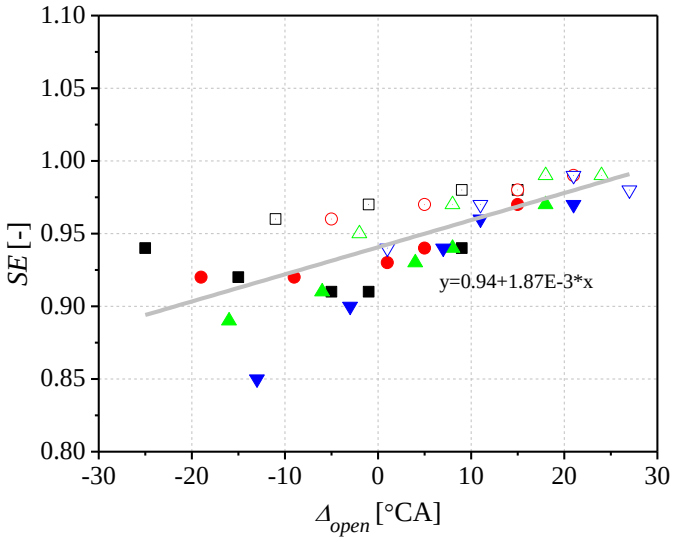

Fig. 34. Correlation of SE with Δ_{open}.

The correlation of CE with Δ_{close} is slightly sensitive to ED, as shown in Fig 35. With the increase in Δ_{close}, CE increases at first but decreases afterwards for both EDs. A negative

Δ_{close} leads to an early SPC and significantly reduces the main scavenging duration, which shows lower CE. However, with a too late SPC, the enhanced post backflow also reduces the CE. Generally speaking, the Δ_{close} should be controlled at the range between 5 and 25 °CA for the EDs in this study to impose the post-charging effect and improves scavenging performances.

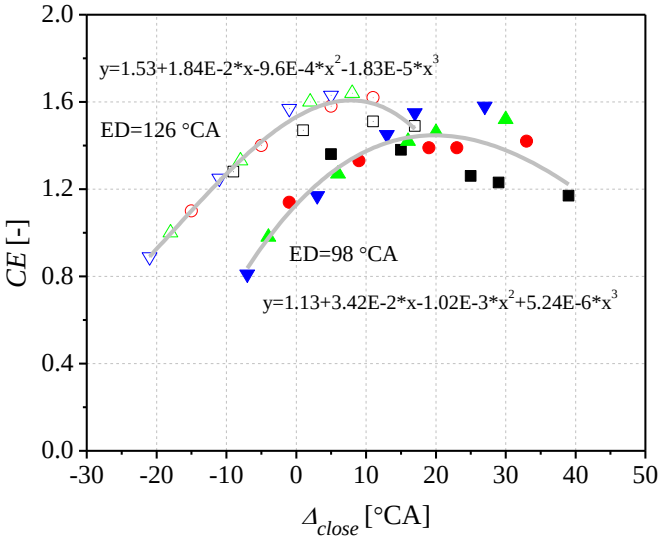

Fig. 35. Correlation of CE with Δ_{close}.

Fig. 36 summarizes the impact of scavenge port/exhaust valve opening profiles on scavenging periods, in-cylinder flow motions and scavenging performances based on the above analyses. In general, Δ_{open} should be increased to increase SE to maximize the scavenge performances. Both Δ_{close} and $\Delta_{overlap}$ should be reduced for the cases with the post backflow and increased for the cases without backflow to improve DR, CE and SE. Therefore, the optimal scavenging performance would be achieved when the post backflow is just avoided by tuning Δ_{close} and $\Delta_{overlap}$ for a specific ED. The prolonged ED could then be used to further improve the scavenging performances, as shown in Fig. 28 and 35.

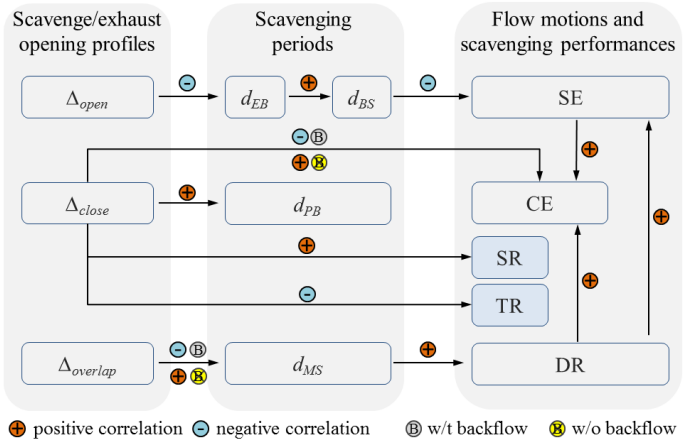

Fig. 36. Mechanism of the effect of scavenge port/exhaust valve opening profiles on scavenging periods, in-cylinder flow motions and scavenging performances.

5. Summary and conclusions

In this study, the three dimensional (3D) computational fluid dynamics (CFD) simulations were performed to understand the effect of scavenge port designs and exhaust valve opening profiles on the in-cylinder flow motions and scavenge performances in a 2-stroke boosted uniflow scavenged direct injection gasoline (BUSDIG) engine. Four scavenging periods, i.e. early backflow period (EB), backflow scavenging period (BS), main scavenging period (MS) and post backflow period (PB), are introduced to characterize the scavenging process and their relationships are analysed with different combinations of scavenge port opening duration (SD), exhaust valve opening duration (ED) and timing (EVO). The main findings are summarized as follows:

1) The delivery ratio (DR) and charging efficiency (CE) gradually increase with the axis inclination angle (AIA) due to the larger effective scavenging area but weakened short-circuiting. The scavenging efficiency (SE) is almost kept constant as AIA increases. The intermediate AIAs of 68° and 75° produce slightly lower swirl ratio (SR) but higher tumble ratio (TR) and cross tumble ratio (CTR).

2) DR is gradually reduced with increasing swirl orientation angle (SOA) due to the reduced effective scavenging area. CE peaks at the intermediate SOAs around 10° and 20° due to less short-circuiting. SE reduces with SOA increasing due to reduced DR and poor scavenging in cylinder centre, while the trapping efficiency (TE) increases slightly. The SR, TR and CTR increase with SOA.
3) The optimal scavenge port angles with AIA of 90° and SOA of 20° produce the best scavenging performances and good in-cylinder flow motions.
4) SR decreases with reduced SD but larger ED, and it is less sensitive to the EVO timing. The intermediate SD (i.e. 110 °CA) and longer ED of 126 °CA produce higher maximum TR. With the decrease of SD and ED, TR shows higher sensitivity to the EVO timing. The shortest SD of 104 °CA generates a higher maximum CTR for both EDs.
5) A longer ED shows lower sensitivity to EVO timing and produces highest maximum DR, SE and CE with an intermediate SD around 110 ^{0}CA. A shorter ED achieves higher TE, and the scavenging performances can be improved with a reduced SD.
6) The increased difference between the opening timings of scavenge ports and exhaust valves (Δ_{open}) leads to reduced early backflow duration (d_{EB}) and the subsequent backflow scavenging duration (d_{BS}), which in turn increases the SE. The increased difference between the closing timings of scavenge ports and exhaust valves (Δ_{close}) leads to increased post backflow duration (d_{PB}) and should be controlled in the range between 5 and 25 ^{0}CA for the EDs in this study to impose the post-charging effect and improves scavenging performances. Meanwhile, Δ_{close} shows strong positive correlation with SR and negative correlation with TR.
7) For the cases with the post backflow, the increase in the overlap between the opening profiles of scavenge ports and exhaust valves ($\Delta_{overlap}$) leads to a shorter main

scavenging duration (d_{MS}). While for those cases without the post backflow, the increased $\Delta_{overlap}$ leads to longer d_{MS}. The adoption of a longer ED can further increase d_{MS}. Overall, DR, SE and CE show strong correlations and increase with d_{MS}.

8) SE and CE show positive correlations with DR. But the correlation between CE and DR is sensitive to ED. A shorter ED is preferred to achieve a higher CE with the same DR. CE shows a positive correlation with SE and shows higher values for a shorter ED.
9) The slopes of the opening profiles of the scavenge ports and the exhaust valve affect both d_{EB} and d_{BS} and the overall scavenging performances.
10) The optimal scavenging performance with higher DR, CE and SE can be achieved when the post backflow is just avoided by tuning the Δ_{close} and $\Delta_{overlap}$ for a specific ED. A longer ED can be used to further improve the scavenging performances. In addition, Δ_{open} can be increased to improve SE.

Abbreviations

3D	three dimensional
AIA	axis inclination angle
BS	backflow scavenging period
BUSDIG	boosted uniflow scavenged direct injection gasoline
CE	charging efficiency
CFD	computational fluid dynamics
CTR	cross tumble ratio
DI	direct injection
DR	delivery ratio
EB	early backflow period

ED	exhaust valve opening duration
EL′	normalized exhaust valve lift
EVO	exhaust valve opening
IMEP	indicated mean effective pressure
MS	main scavenging period
PB	post backflow period
RGF	residual gas fraction
SA′	normalized scavenge port opening area
SD	scavenge port opening duration
SE	scavenging efficiency
SOA	swirl orientation angle
SPC	scavenge port closing
SPO	scavenge port opening
SR	swirl ratio
TDC	top dead center
TE	trapping efficiency
TR	tumble ratio
VVA	variable valve actuation

Notations

Δ_{close}	difference between the closing timings of scavenge ports and exhaust valves
$\Delta_{overlap}$	overlap between the opening profiles of scavenge ports and exhaust valves
Δ_{open}	difference between the opening timings of scavenge ports and exhaust valves
δ	changing percentage
d	duration

Funding

The authors gratefully acknowledge the financial support by the Engineering and Physical Sciences Research Council (EPSRC). The data of this paper can be accessed from the Brunel University London data archive, figshare at https://doi.org/10.17633/rd.brunel.5195731.v1.

Reference

[1] Mattarelli E, Rinaldini C A. Two-Stroke Gasoline Engines for Small-Medium Passenger Cars. SAE Technical Paper 2015-01-1284.

[2] Zhang Y, Nora M D, Zhao H. Comparison of Performance, Efficiency and Emissions between Gasoline and E85 in a Two-Stroke Poppet Valve Engine with Lean Boost CAI Operation. SAE Technical Paper 2015-01-0827.

[3] Nishida K, Sakuyama H, Kimijima T. Improvement of Fuel Economy Using a New Concept of Two-Stroke Gasoline Engine Applying Stratified-Charge Auto-Ignition. SAE Technical Paper 2009-28-0009.

[4] Johnson J, Den Braven K R. Comparison of Homogeneous, Stratified and High-Squish Stratified Combustion in a Direct-Injected Two-Stroke Engine. SAE Technical Paper 2008-32-0030.

[5] Osborne R J, Stokes J, Lake T H, Carden P J, Mullineux J D, Helle-Lorentzen R, Evans J C, Heikal M R, Zhu Y, Zhao H, Ma T. Development of a Two-Stroke/Four-Stroke Switching Gasoline Engine - The 2/4SIGHT Concept. SAE Technical Paper 2005-01-1137.

[6] Zhang Y, Zhao H, Ojapah M, Cairns A. 2-Stroke CAI Operation on a Poppet Valve DI Engine Fuelled with Gasoline and its Blends with Ethanol. SAE Technical Paper 2013-01-1674.

[7] Benajes J, Martin J, Novella R, De Lima D. Analysis of the Load Effect on the Partially Premixed Combustion Concept in a 2-Stroke HSDI Diesel Engine Fueled with Conventional Gasoline. SAE Technical Paper 2014-01-1291.

[8] Andwari A M, Aziz A A, Said M F M, Latiff Z A. Experimental investigation of the influence of internal and external EGR on the combustion characteristics of a controlled auto-ignition two-stroke cycle engine. Applied Energy 2014; 134(0): 1 - 10.

[9] Rocchi S, Rossi R, Musu E, Gentili R, Ghandhi J, Reitz R D. Computational study of a two-stroke direct-injection reactivity-controlled compression ignition engine. Proceedings of the Institution of Mechanical Engineers, Part D: Journal of Automobile Engineering 2014; 229(8): 980–991.

[10] Benajes J, Novella R, De Lima D, Tribotte P. Investigation on Multiple Injection Strategies for Gasoline PPC Operation in a Newly Designed 2-Stroke HSDI Compression Ignition Engine. SAE Int. J. Engines 2015; 8(2).

[11] Zhang Y, Zhao H. Measurement of short-circuiting and its effect on the controlled autoignition or homogeneous charge compression ignition combustion in a two-stroke poppet valve engine. Proceedings of the Institution of Mechanical Engineers, Part D: Journal of Automobile Engineering 2012; 226(8): 1110-1118.

[12] Abthoff J, Duvinage F, Hardt T, Krämer M, Paule M. The 2-Stroke DI-Diesel Engine with Common Rail Injection for Passenger Car Application. SAE Technical Paper 981032.

[13] Lamas M I, Vidal R, Gervasio C. Computational Fluid Dynamics Analysis of the Scavenging Process in the MAN B&W 7S50MC Two-Stroke Marine Diesel Engine. Journal of Ship Research 2012; 56(3): 154-161(8).

[14] Sigurdsson E, Ingvorsen K M, Jensen M V, Mayer S, Matlok S, Walther J H. Numerical analysis of the scavenge flow and convective heat transfer in large two-stroke marine diesel engines. Applied Energy 2014; 123(0): 37 - 46.

[15] Andersen F H, Hult J, Nogenmyr K, Mayer S. CFD Analysis of the Scavenging Process in Marine Two-Stroke Diesel Engines. Proceedings of the ASME 2014 Internal Combustion Engine Division Fall Technical Conference, October 19-22, 2014, Columbus, IN, USA.

[16] Knoll R. AVL Two-Stroke Diesel Engine. SAE Technical Paper 981038.

[17] Cantore G, Mattarelli E. A New Concept for Ultra-Compact Automotive HSDI Diesel Engines. SAE Technical Paper 2007-01-1253.

[18] Laget O, Ternel C, Thiriot J, Charmasson S, Tribotté P, Vidal F. Preliminary Design of a Two-Stroke Uniflow Diesel Engine for Passenger Car. SAE Int. J. Engines 2013; 6(1).

[19] Mattarelli E, Rinaldini C A, Baldini P. Modeling and Experimental Investigation of a 2-Stroke GDI Engine for Range Extender Applications. SAE Technical Paper 2014-01-1672.

[20] Ingvorsen K M, Meyer K E, Walther J H, Mayer S. Turbulent swirling flow in a dynamic model of a uniflow-scavenged two-stroke engine. Experiments in Fluids 2014; 55(6).

[21] Ingvorsen K M, Meyer K E, Walther J H E, Mayer S. Phase-locked stereoscopic PIV measurements of the turbulent swirling flow in a dynamic model of a uniflow-scavenged two-stroke engine cylinder. 10TH INTERNATIONAL SYMPOSIUM ON PARTICLE IMAGE VELOCIMETRY, Delft, The Netherlands, July 1-3, 2013.

[22] Haider S, Schnipper T, Obeidat A, Meyer K E, Okulov V L, Mayer S, Walther J H. PIV study of the effect of piston position on the in-cylinder swirling flow during the scavenging process in large two-stroke marine diesel engines. Journal of Marine Science and Technology 2013; 18(1): 133-143.

[23] Hori H. Scavenging Flow Optimization of Two-Stroke Diesel Engine by Use of CFD. SAE Technical Paper 2000-01-0903.

[24] Tamamidis P, Assanis D N. Optimization of inlet port design in a uniflow-scavenged engine using a 3-D turbulent flow code. SAE Technical Paper 931181.

[25] Ravi M R, Marathe A G. Effect of port sizes and timings on the scavenging characteristics of a uniflow scavenged engine. SAE Technical Paper 920782.

[26] Carlucci A P, Ficarella A, Trullo G. Performance optimization of a Two-Stroke supercharged diesel engine for aircraft propulsion. Energy Conversion and Management 2016; 122: 279-289.

[27] Ma J, Zhao H. The Modeling and Design of a Boosted Uniflow Scavenged Direct Injection Gasoline (BUSDIG) Engine. SAE Technical Paper 2015-01-1970.

[28] Wang X, Ma J, Zhao H. Evaluations of Scavenge Port Designs for a Boosted Uniflow Scavenged Direct Injection Gasoline (BUSDIG) Engine by 3D CFD Simulations. SAE Technical Paper 2016-01-1049.

[29] Cd-adapco. Methodology, STAR-CD VERSION 4.14, 2010.

[30] Ma J, Zhao H, Freeland P, Hawley M, Xia J. Numerical Analysis of a Downsized 2-Stroke Uniflow Engine. SAE Technical Paper 2014-01-9051.

[31] Wang X, Xie H, Zhao H. Computational study of the influence of in-cylinder flow on spark ignition–controlled auto-ignition hybrid combustion in a gasoline engine. International Journal of Engine Research 2015; 16(5): 795-809.